Available online at www.sciencedirect.com
SCIENCE DIRECT
Bioorganic & Medicinal Chemistry
Bioorganic & Medicinal Chemistry 14 (2006) 1462–1473

Understanding the structure–activity and structure–selectivity correlation of cyclic guanine derivatives as phosphodiesterase-5 inhibitors by molecular docking, CoMFA and CoMSIA analyses

Guang-Fu Yang,* Hai-Ting Lu, Ying Xiong and Chang-Guo Zhan*

Key Laboratory of Pesticide and Chemical Biology of Ministry of Education, College of Chemistry, Central China Normal University, Wuhan 430079, PR China
Department of Pharmaceutical Sciences, College of Pharmacy, University of Kentucky, 725 Rose Street, Lexington, Kentucky 40536, USA

Received 7 September 2005; revised 29 September 2005; accepted 29 September 2005
Available online 2 November 2005

Abstract—Molecular docking and 3D-QSAR analyses were performed to understand how PDE5 and PDE6 interact with a series of (49) cyclic guanine derivatives. Using the conformations of the compounds revealed by molecular docking, CoMFA and CoMSIA analyses resulted in the first quantitative structure–activity relationship (QSAR) and first quantitative structure–selectivity relationship (QSSR) models (with high cross-validated correlation coefficient q^2 and conventional correlation coefficient r^2 values) for predicting the inhibitory activity against PDE5 and the selectivity against PDE6. The high q^2 and r^2 values, along with further testing, indicate that the obtained 3D-QSAR and 3D-QSSR models will be valuable in predicting both the inhibitory activity and selectivity of cyclic guanine derivatives for these protein targets. A set of 3D contour plots drawn based on the 3D-QSAR and 3D-QSSR models reveal some useful clues to improve both the activity and selectivity by modifying structures of the compounds. It has been demonstrated that both the steric and electrostatic factors should appropriately be taken into account in future rational design and development of more active and more selective PDE5 inhibitors for the therapeutic treatment of erectile dysfunction (ED).

1. Introduction

Phosphodiesterases (PDEs) are a superfamily of enzymes responsible for the hydrolysis of 3′,5′-cyclic monophosphate (cAMP) and cyclic guanosine 3′,5′-monophosphate (cGMP) that are important intracellular second messengers playing a central role in regulating many relevant cell functions.[1–5] Among the 11 different PDE families (PDE1 to PDE11) identified and characterized so far, PDE5 is the primary target for the development of small molecules, as PDE5 inhibitors, to treat male erectile dysfunction (ED).[6–9] Upon sexual stimulation, nitric oxide (NO) is released from non-adrenergic, non-cholinergic neurons in the penis.[10,11] NO activates guanylyl cyclase, which in turn produces cGMP. cGMP initiates a protein phosphorylation cascade, which causes a decrease in intracellular calcium within *corpus cavernosum* smooth muscle cells, resulting in vasorelaxation, inflow of arterial blood, and erection. Inhibition of PDE5 increases the effective concentration of cGMP in the *corpus cavernosum*, enhancing the above-described effects.

The development of PDE5 inhibitors for the therapeutic treatment of ED has attracted great attention since the commercial introduction of sildenafil (Viagra) in 1998 and other two commercial PDE5 inhibitors, that is, vardenafil (Levitra) and tadalafil (Cialis), in 2003.[12–19] Despite their commercial success, the PDE5 inhibitors in clinical use have shown significant side effects, most of which are related to the insufficient selectivity versus other PDEs, specially reported incidences of visual disturbances may be linked to the unexpected inhibition of PDE6.[20] So, both the inhibitory activity and selectivity should be paid the same attention in the design of new PDE5 inhibitors for therapeutic use. This requires insights into the factors that influence the activity and selectivity of PDE5 inhibitors to guide future rational drug design. Although X-ray crystal structures of the

Keywords: Phosphodiesterase; Enzyme; Inhibitor; Binding mode; Selective inhibition; Structure–activity correlation.
* Corresponding authors. Tel.: +1 8593233943; fax: +1 8593233575 (C.-G.Z.); e-mail addresses: gfyang@mail.ccnu.edu.cn; zhan@uky.edu

0968-0896/$ - see front matter © 2005 Elsevier Ltd. All rights reserved.
doi:10.1016/j.bmc.2005.09.073

catalytic domain of human PDE5 with drug molecules bound in the active site cavity were determined recently,[21,22] there is still no X-ray crystal structure available for the catalytic domain or binding site of PDE6. A deep understanding of the structure–activity and structure–selectivity correlation is crucial for future rational design of novel PDE5 inhibitors with the desirable higher activity and higher selectivity.

Nowadays, three-dimensional (3D) quantitative structure–activity relationship (3D-QSAR) techniques, such as comparative molecular field analysis (CoMFA) and comparative molecular similarity analysis (CoMSIA),[23–28] are routinely used in modern drug design to help understand drug–receptor interaction. It has been shown in the literature that these computational techniques can strongly support and help the design of novel, more potent inhibitors by revealing the mechanism of drug–receptor interaction.[29–31] However, so far, there has been no report concerning the application of a QSAR methodology to the activity or selectivity of PDE5 inhibitors. In addition to the QSAR, understanding the quantitative structure–selectivity relationship (QSSR) is also crucial for the development of these inhibitors.

Here we report the first QSAR and QSSR study on PDE5 inhibitors, along with molecular docking modeling of the protein-inhibitor binding. Cyclic guanine derivatives, that have attracted much attention in recent years,[32–34] have been identified as a novel kind of PDE5 inhibitors with good selectivity and were chosen as a target scaffold in this study. To investigate the mode of recognition and interaction of these PDE5 inhibitors and to design new PDE5 inhibitors with possibly higher inhibitory activity and higher selectivity, we have performed molecular docking and 3D-QSAR and 3D-QSSR analyses on these cyclic guanine derivatives interacting with PDE5. The topographical features of PDE5 and PDE6 active sites can be discussed based on the obtained 3D-QSAR and 3D-QSSR models. The satisfactory quantitative structure–activity and structure–selectivity correlation relationships obtained provide a solid basis for future rational design of more active and more selective inhibitors of PDE5 within the family of cyclic guanine derivatives.

2. Computational details

2.1. Data sets

All compounds examined in the present study were reported recently by Pissarnitski and co-workers.[34] Within a total of 59 compounds reported, 10 compounds are discarded, because the IC_{50} (i.e., the concentration causing 50% inhibitory effect) values are not available for these 10 compounds. The training set consisting of 37 compounds and test set consisting of 12 compounds were randomly selected from the remaining 49 compounds with the IC_{50} values against PDE5 and PDE6. An attractive feature of these compounds is their relative conformational rigidity, which makes them more amenable to meaningful CoMFA and CoMSIA analyses than flexible molecules. The IC_{50} values were converted to pIC_{50} (i.e., $-\log IC_{50}$) values. The log of the reported IC_{50}(PDE6/5) value, that is, $\log IC_{50}$(PDE6/5), can be used as an index for the selectivity (PDE6/5). The pIC_{50}(PDE5) and $\log IC_{50}$(PDE6/5) values of the compounds from the training and test sets covered an interval of more than 3 log units for the inhibitory activity and selectivity against the target enzymes.

2.2. Molecular docking

AutoDock 3.0 program suite[35] was used to perform automated docking of three representative flexible ligands (compounds **8**, **9**, and **20** in Table 1) into the PDE5 binding site by using the Lamarckian genetic algorithm (LGA) method and a recently reported X-ray crystal structure of the catalytic domain of PDE5A.[22] In the reported X-ray crystal structure, the PDE5 active site contains a cluster of two divalent metal ions, denoted by Me1 and Me2. Me1 should be a Zn^{2+} ion based on the observed geometry of the metal coordinating ligands, the anomalous X-ray diffraction behavior, the existing biochemical evidence, and the known high affinity of PDE for zinc and Me2 is most likely Mg^{2+}. According to the 3D X-ray crystal structure, there are two ligands bridging the two metal ions. One bridging ligand is clearly an Asp residue whose two O_δ atoms, respectively, coordinate Me1 and Me2. However, it was uncertain whether the second bridging ligand (BL2) should be a water molecule or a hydroxide ion, since hydrogen atoms cannot be determined by the X-ray diffraction techniques.[36–39] Nevertheless, in light of our previously reported computational evidence concerning the PDE active site structures,[40] BL2 should be a hydroxide ion, rather than a water molecule. Starting from the original pdb file of the X-ray crystal structure,[22] all hetero atoms were removed except the protein atoms, along with the metal ions, the bridging hydroxide ion, and water molecules coordinating the metal ions. Polar hydrogen atoms were added and Kollman united-atom charges were assigned on the PDE5A enzyme.

The parameters for the metal ions must be defined before one can carry out molecular docking with a metalloenzyme. We used the van der Waals parameters ($r = 1.1$ Å and $\varepsilon = 0.25$ kcal/mol) developed by Stote and Karplus[41] for Zn^{2+} (with a charge of +2.0), as we did in our previous MD simulations of other Zn^{2+}-containing protein–ligand systems.[36–39] For Mg^{2+} (with a charge of +2.0), we used the van der Waals parameters ($r = 0.7926$ Å and $\varepsilon = 0.8947$ kcal/mol) provided in the AMBER7 program suite.[42] In addition, the atomic charges on the oxygen and hydrogen atoms of the bridging hydroxide ion were set to −1.207 and 0.207, respectively, that are the electrostatic-potential (ESP) fitted charges determined by performing ab initio molecular orbital calculation on the hydroxide ion using Gaussian03 program[43] at the HF/6-31G* level.

The PDE5 active site was defined by using the AutoGrid module of the AutoDock 3.0 program suite. The grid

Table 1. Molecular structures of the compounds in the training and test sets

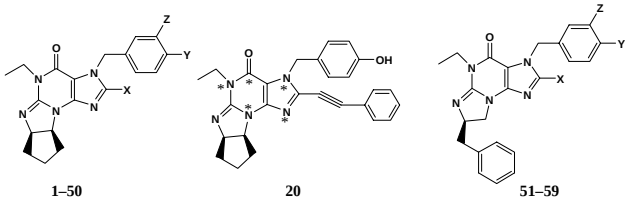

Compound	X	Y	Z
1	CH_2-Ph	H	H
2	CH_2-Ph	*p*-Me	H
5	CH_2-Ph	*p*-Cl	H
15	CH_2-Ph	*p*-Me, *m*-Cl	Cl
16	CH_2-Ph	3,4-Methylenedioxy	
18	CCPh	*p*-Cl	H
19	CCPh	*p*-MeO	H
20	CCPh	*p*-OH	H
25	OEt	MeO	H
26	SEt	MeO	H
27	COOMe	MeO	H
28	CN	MeO	H
29	$CONH_2$	MeO	H
31	CF_3	OH	H
32	$CONH_2$	OH	H
33	SEt	OH	H
36	H	MeO	Br
37	H	MeO	Cl
39	$CONH_2$	MeO	Br
40	$CONH_2$	OH	Br
41	$CONH_2$	OH	Cl
42	CONHMe	MeO	Cl
43	CONHMe	OH	Cl
44	OEt	MeO	Br
45	OEt	MeO	Cl
46	OEt	OH	Cl
47	OMe	MeO	Br
48	OMe	MeO	Cl
49	OMe	OH	Br
50	OMe	OH	Cl
51	$CONH_2$	MeO	Cl
52	$CONH_2$	OH	Cl
53	OBn	OH	Cl
54	OMe	MeO	CN
55	OMe	MeO	Br
58	OMe	OH	Br
59	OMe	OH	Cl
7[a]	CH_2-Ph	*p*-MeO	H
8[a]	CH_2-Ph	*p*-OH	H
9[a]	CH_2-Ph	*p*-NH_2	H
17[a]	CCPh	H	H
23[a]	H	MeO	H
24[a]	CF_3	MeO	H
30[a]	NH_2	OH	H
34[a]	OEt	OH	H
35[a]	N_3	OH	H
38[a]	H	OH	Br
56[a]	OMe	MeO	Cl
57[a]	OMe	OH	CN

[a] Compounds in the test set.

size was set to $120 \times 120 \times 120$ points with a grid spacing of 0.375 Å centered on the active site of the crystal structure. The grid box includes almost the entire enzyme and provides enough space for the translational and rotational walk of the ligand. Fifty runs were performed for docking with each ligand. For each of the 50 independent runs, a maximum number of 27,000 GA operations were generated on a single population of 50 individuals. The operator weights used for crossover rate, mutation rate, and elitism value were the default parameters 0.80, 0.02, and 1, respectively.

2.3. 3D-QSAR and 3D-QSSR analyses

The 3D structures of all compounds were built by using SYBYL 7.0 on a Silicon Graphics Fuel workstation. The molecular conformation of compound **20** obtained from the molecular docking was used as a template to build molecular structures of all the compounds. Then, the built molecular structures were superimposed using the Alignment database command. The common substructure consisting of asterisked atoms in compound **20**, including the four aromatic nitrogen atoms and a carbonyl carbon atom (see Table 1), was used for aligning the molecular structures. Atomic charges were calculated using PM3 semiempirical molecular orbital method implemented in the MOPAC program interfaced with SYBYL.

The CoMFA descriptors, steric and electrostatic field energies, were calculated using the SYBYL default parameters: 2 Å grid points spacing, an sp^3 carbon probe atom with +1 charge and a minimum σ (column filtering) of 2.0 kcal/mol, and an energy cutoff of 30 kcal/mol.

The alignment was also used to calculate similarity index fields for CoMSIA analysis. The five similarity indices in CoMSIA, that is, the steric (S), electrostatic (E), hydrophobic (H), H-bond donor (D), and H-bond acceptor (A) descriptors, were calculated using a $C1^+$ probe atom with a radius of 1.0 Å placed at regular grid spacing of 2 Å. CoMSIA similarity indices (A_F) for a molecule j with atom i at a grid point q are calculated by Eq. 1:

$$A_{F,k}^{q}(j) = -\sum \omega_{probe,k}\omega_{ik}e^{-\alpha r_{iq}^2}, \quad (1)$$

where k represents the steric, electrostatic, hydrophobic, H-bond donor, or H-bond acceptor descriptor. A Gaussian type distance-dependence was used between the grid point q and each atom i of the molecule. The default value of 0.3 was used as the attenuation factor (α). Here, the steric indices are related to the third power of the atomic radii, electrostatic descriptors are derived from partial atomic charges, hydrophobic fields are derived from atom-based parameters, and H-bond donor and acceptor indices are obtained by a rule-based method based on experimental results.

The CoMFA and CoMSIA descriptors derived were used as explanatory variables, and pIC_{50}(PDE5) and $\log IC_{50}$(PDE6/5) were used as the target variables in PLS regression analyses to derive 3D-QSAR and 3D-QSSR models using the implementation in the SYBYL package. The predictability of the models was evaluated by performing the leave-one-out (LOO) cross-valida-

tion. The cross-validation correlation coefficient, q^2, was calculated by using Eq. 2:

$$q^2 = 1 - \frac{\sum(Y_{\text{predicted}} - Y_{\text{observed}})^2}{\sum(Y_{\text{observed}} - Y_{\text{mean}})^2}, \quad (2)$$

where $Y_{\text{predicted}}$, Y_{observed}, and Y_{mean} are predicted, observed, and mean values of the target property (pIC_{50}(PDE5) or $\log IC_{50}$(PDE6/5)), respectively. $\sum(Y_{\text{predicted}} - Y_{\text{observed}})^2$ is the predicted sum of squares (PRESS). To maintain the optimum number of PLS components and avoid over-training, the number of components giving the lowest PRESS value was used to derive the final PLS regression models. Conventional correlation coefficient, r^2, and its standard error, s, were also computed for the final PLS models. CoMFA and CoMSIA coefficient maps were generated by interpolation of the pairwise products between the PLS coefficients and the standard deviations of the corresponding CoMFA or CoMSIA descriptor values.

3. Results and discussion

3.1. PDE5-ligand binding and conformation of the ligand

Depicted in Figure 1 are the most stable structures for PDE5 binding with compounds **8**, **9**, and **20** obtained from the molecular docking. We carried out the docking with these three particular compounds because compound **20** is associated with the lowest IC_{50}(PDE5) value, compound **9** is associated with the highest

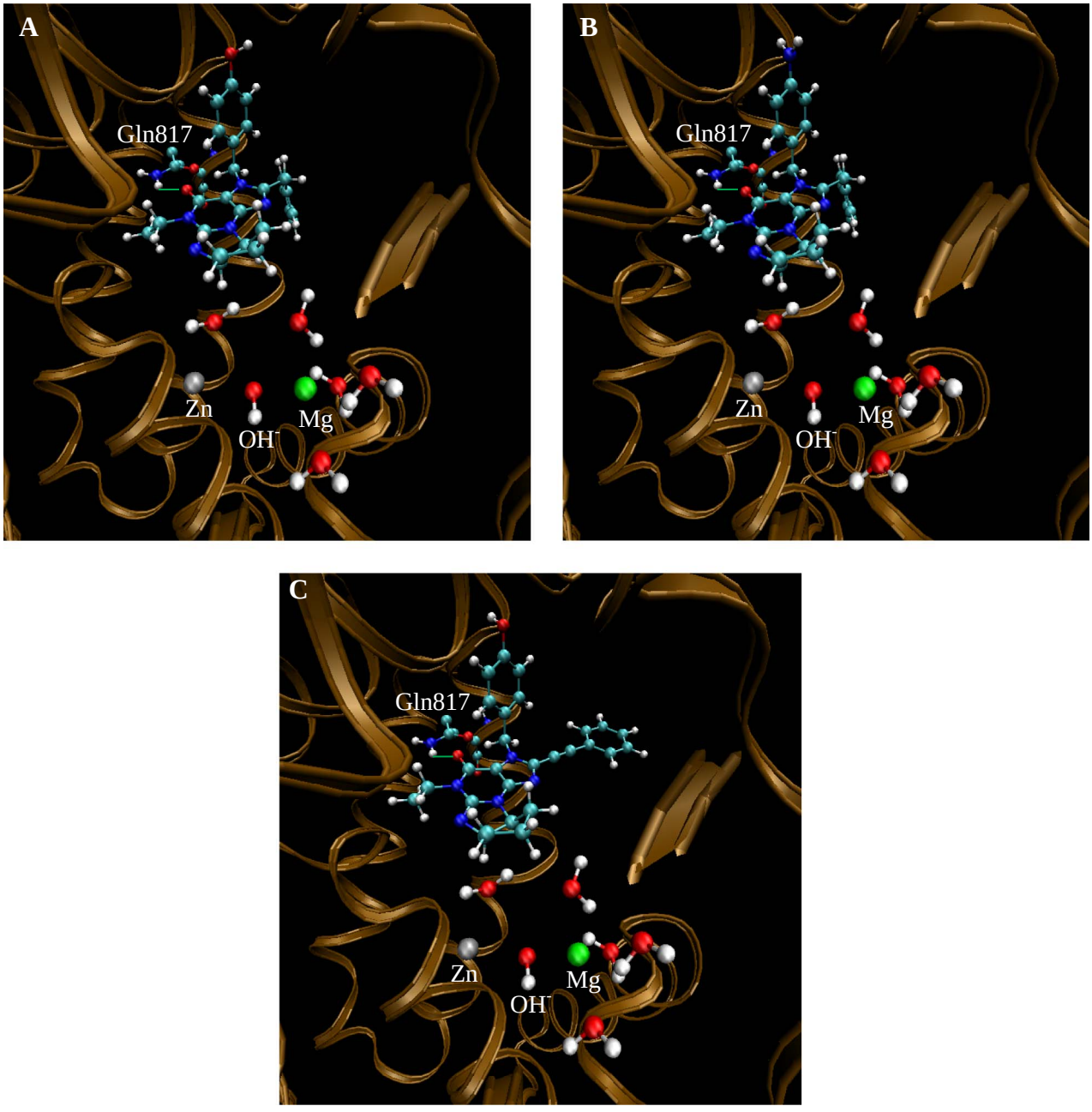

Figure 1. Structures of PDE5 binding with compounds **8** (A), **9** (B), and **20** (C) obtained from molecular docking with AutoDock 3.0 program.

IC_{50}(PDE5) value, and compound **8** is associated with a middle IC_{50}(PDE5) value. A survey of the binding structures depicted in Figure 1 reveals that these three compounds bind to PDE5 very similarly, providing a rational structural basis for our 3D-QSAR and 3D-QSSR analyses. A remarkable feature of the PDE5-ligand binding structures in Figure 1 is a common hydrogen bond between the nitrogen of the amine group of the Glu817 side chain and the carbonyl oxygen of the ligand. This hydrogen bond exists in all of the docked PDE5-ligand binding structures.

3.2. 3D-QSAR and -QSSR models

3.2.1. CoMFA model. CoMFA was developed to model the protein–ligand interactions based on standard steric and electrostatic molecular fields to model the protein–ligand interactions. Despite being unable to describe all of the binding forces, CoMFA is still a widely used tool for a QSAR analysis at 3D level. The major objective of the CoMFA analysis is to find the best predictive model within the system. PLS analysis results for the pIC_{50}(PDE5) values are listed in Table 2. For convenience, the models obtained for the PDE5 inhibitory activity and for the selectivity between PDE6 and PDE5 will be named the pIC_{50}(PDE5) and $\log IC_{50}$(PDE6/5) models, respectively. As summarized in Table 2, a CoMFA model with a cross-validation q^2 value of 0.755 for six components was obtained for the inhibitory activity characterized by pIC_{50}(PDE5), whereas a model with the q^2 value of 0.832 for five components was obtained for the selectivity characterized by $\log IC_{50}$(PDE6/5). The non-cross-validated PLS analyses were repeated with the optimum number of components, as determined by the cross-validation analysis, to give $r^2 = 0.932$ and 0.955 for the pIC_{50}(PDE5) and $\log IC_{50}$(PDE6/5) models, respectively. These correlation coefficients suggest that both the pIC_{50}(PDE5) and $\log IC_{50}$(PDE6/5) models are reliable and accurate. The inhibitory activity values predicted for these compounds are listed in Table 3 and depicted in Figures 2A and B.

3.2.2. CoMSIA model. Comparative molecular similarity indices analysis (CoMSIA) computes the steric and electrostatic fields, as in CoMFA, but it also computes additional hydrophobic, hydrogen-bond donor, and hydrogen-bond acceptor fields. The resulting field contour maps are easier to interpret than those in CoMFA, since a Gaussian function is used to determine the distance-dependence. Therefore, the similarity indices can also be calculated CoMSIA at the grid points inside the molecules, not just outside, as with CoMFA.[27] CoMSIA, in most instances, performs similarly to CoMFA in terms of predictive ability. It is a valuable addition to the 3D-QSAR tool kit and CoMSIA is gaining popularity. In the present study, we obtained better PLS statistics and predictive performance on the test set with the CoMSIA 3D-QSAR and QSSR models than that with the CoMFA models. The results of the initial CoMSIA models for different combinations are summarized in Table 2. For both pIC_{50}(PDE5) and $\log IC_{50}$(PDE6/5), the CoMSIA models with q^2 values of over 0.79 were obtained, indicating that the obtained CoMSIA models should be more accurate than the corresponding CoMFA models in predicting the inhibitory activity of cyclic guanines against PDE5. The model obtained for $\log IC_{50}$(PDE6/5) performs significantly better than the corresponding model obtained for pIC_{50}(PDE5) based on the obtained q^2 and r^2 values. For pIC_{50}(PDE5), a combined use of the steric, electrostatic, and hydrogen-bond acceptor descriptors resulted in the best model ($q^2 = 0.791$ and $r^2 = 0.941$ with six components). For $\log IC_{50}$(PDE6/5), a combined use of the steric, electrostatic, hydrophobic, and hydrogen-bond acceptor descriptors produced the best model ($q^2 = 0.869$ and $r^2 = 0.946$ with four components).

3.2.3. Validation of the 3D-QSAR and -QSSR models. As seen in Table 3, the trained CoMSIA models can reproduce the experimental data very well for both the pIC_{50}(PDE5) and $\log IC_{50}$(PDE6/5) values of all the compounds included in the training set. The ultimate test for the predictability of a QSAR or QSSR model in the drug design process is to predict the biological activity/selectivity of new compounds that are not included in the training set. The 3D-QSAR and 3D-QSSR models obtained in this study were challenged with a test set consisting of 12 randomly selected compounds. The compounds in this test set include cyclic guanines representing structures similar to those of the training

Table 2. Summary of the 3D-QSAR and 3D-QSSR models[a]

PLS statistic	pIC_{50} (PDE5) model				$\log IC_{50}$ (PDE6/5) model			
	CoMFA	CoMSIA			CoMFA	CoMSIA		
	SE	SEHDA	SEHA	SEA	SE	SEHDA	SEHA	SEA
q^2_{cv}	0.755	0.787	0.788	0.791	0.832	0.858	0.869	0.868
Number of components	6	4	3	6	5	4	4	4
r^2_{ncv}	0.932	0.915	0.887	0.941	0.955	0.930	0.946	0.935
s	0.172	0.185	0.210	0.160	0.205	0.252	0.220	0.243
F	68.080	86.153	86.250	79.244	131.251	106.341	140.844	114.852
Field contribution								
Steric	0.499	0.093	0.110	0.199	0.575	0.090	0.093	0.166
Electrostatic	0.501	0.209	0.213	0.467	0.425	0.226	0.239	0.441
Hydrophobic		0.345	0.388			0.311	0.345	
Donor		0.273				0.227		
Acceptor		0.080	0.289	0.334		0.146	0.322	0.392

[a] S, steric; E, electrostatic; H, hydrophobic; D, donor; A, acceptor.

Table 3. Predictions for the training set

Compound	pIC_{50} (PDE5) models			$\log IC_{50}$(PDE6/5) models		
	Observed	Predicted		Observed	Predicted	
	pIC_{50}	CoMFA	CoMSIA[a]	$\log IC_{50}$	CoMFA	CoMSIA[a]
1	6.89	7.06	6.97	0.41	0.53	0.26
2	7.40	7.14	7.08	0.18	0.12	0.21
5	6.80	7.01	7.05	0.20	0.39	0.36
15	7.24	7.11	7.32	0.83	0.08	0.35
16	7.34	7.31	7.37	−0.16	0.17	0.08
18	8.30	8.59	8.49	0.53	0.49	0.28
19	8.51	8.47	8.60	−0.30	−0.15	−0.12
20	9.52	9.06	9.18	1.01	0.89	0.87
25	7.74	7.90	7.84	0.15	0.35	0.44
26	7.89	7.92	8.00	0.00	0.15	0.25
27	8.17	8.00	8.02	−0.10	−0.11	0.03
28	8.20	8.10	8.14	0.08	0.17	0.07
29	8.40	8.50	8.41	0.48	0.48	0.35
31	8.15	8.32	8.18	1.36	1.28	1.36
32	8.68	8.83	8.70	1.45	1.66	1.43
33	8.74	8.59	8.56	1.40	1.27	1.23
36	8.19	8.11	8.30	0.78	0.76	1.09
37	8.08	8.11	7.97	0.60	0.64	0.80
39	8.82	8.64	8.71	0.97	0.98	1.05
40	9.05	9.04	9.08	1.70	1.65	1.80
41	8.96	8.99	8.91	1.91	1.86	1.81
42	8.64	8.62	8.55	0.81	0.82	0.69
43	8.89	8.98	9.01	1.51	1.69	1.60
44	8.27	8.31	8.51	1.04	0.90	1.08
45	8.19	8.08	8.12	0.90	0.83	0.87
46	8.68	8.63	8.67	1.76	1.54	1.79
47	8.55	8.63	8.58	1.51	1.40	1.24
48	8.30	8.33	8.16	1.00	1.24	1.00
49	8.80	8.86	8.85	2.29	2.06	2.17
50	8.70	8.88	8.77	2.00	2.14	2.00
51	8.55	8.61	8.50	1.79	1.78	1.64
52	8.52	8.79	8.87	2.78	2.70	2.74
53	8.68	8.62	8.77	2.21	2.28	2.37
54	7.96	8.02	7.78	2.65	2.44	2.00
55	8.66	8.42	8.56	2.24	2.17	2.20
58	8.89	8.74	8.78	2.75	2.80	3.04
59	8.72	8.76	8.70	2.62	2.91	2.89

[a] Calculated by using the best CoMSIA model.

set compounds and one derivative with new structural features, for example, compound **35** bearing a N_3 group. The predicted pIC_{50}(PDE5) and $\log IC_{50}$(PDE6/5) values for the test set are summarized in Table 4 and depicted in Figures 2C and D.

A survey of the results in Tables 3 and 4 reveals that the CoMSIA models are better than the corresponding CoMFA models for both pIC_{50}(PDE5) and $\log IC_{50}$(PDE6/5). A closer look at the results indicates that the pIC_{50}(PDE5) and $\log IC_{50}$(PDE6/5) values of compound **57** are overestimated significantly by all of the 3D-QSAR and 3D-QSSR models. Although the pIC_{50}(PDE5) values of compounds **8** and **30** are significantly underestimated or overestimated by the CoMFA model, these pIC_{50}(PDE5) values are predicted much better by the CoMSIA model. In addition, the pIC_{50}(PDE5) value of compound **35**, bearing a N_3 group at *X*-position, was significantly underestimated by the CoMSIA model, which may be explained by the fact that the training set did not include the similar compound which could contribute required information to the model regarding the *X*-position. However, the $\log IC_{50}$(PDE6/5) models predict the selectivity of the compound **35** quite well, indicating that the absence of a comparable compound in the training set is not critical for these compounds. This observation is suggestive of the similarity in the *X*-position binding pocket between PDE5 and PDE6. Except for these specially mentioned compounds, both the inhibitory activity and selectivity, that is, the pIC_{50}(PDE5) and $\log IC_{50}$(PDE6/5) values, of the other compounds in the test set are all predicted reasonably well. Therefore, we believe that these obtained 3D-QSAR and 3D-QSSR models can be used as predictive tools in future rational design of PDE5 inhibitors with the desirable higher activity and higher selectivity.

3.3. Analysis of the 3D contour maps of the best models

In the figures discussed below, the isocontour diagrams of the field contributions ('stdev*coeff') of different

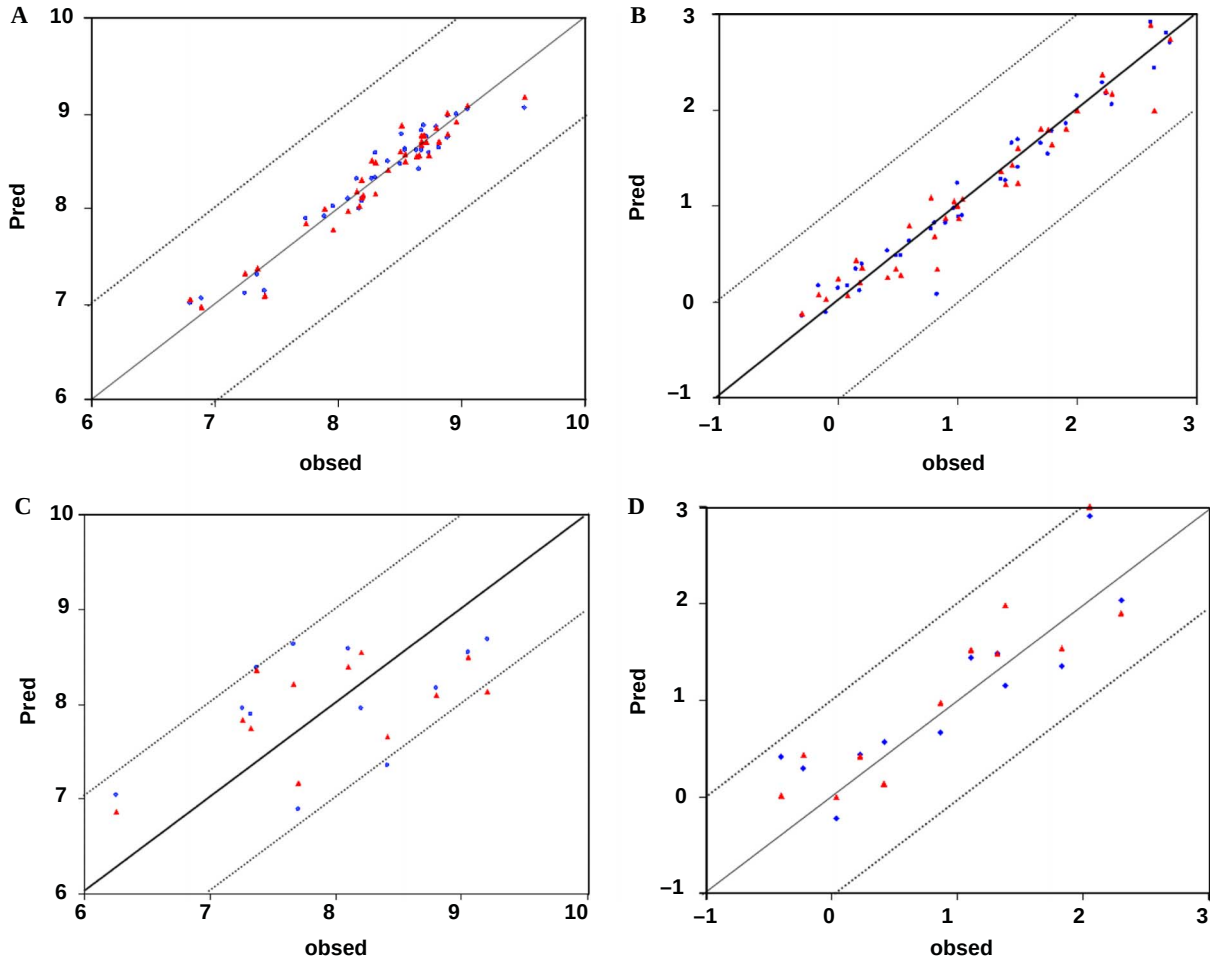

Figure 2. Plots of the predicted pIC_{50} versus observed pIC_{50} (or $\log IC_{50}$) values. Red represents the CoMSIA results, whereas blue refers to the CoMFA results: (A) the pIC_{50}(PDE5) model for the training set; (B) the $\log IC_{50}$(PDE6/5) model for the training set; (C) the pIC_{50}(PDE5) model for the test set; (D) the $\log IC_{50}$(PDE6/5) model for the test set.

Table 4. Predictions for the test set

Compound	pIC_{50}(PDE5) models			$\log IC_{50}$(PDE6/5) models		
	Observed	Predicted		Observed	Predicted	
	pIC_{50}	CoMFA	CoMSIA[a]	$\log IC_{50}$	CoMFA	CoMSIA[a]
7	7.70	6.89	7.17	0.04	−0.22	−0.01
8	8.41	7.35	7.66	0.87	0.66	0.97
9	6.26	7.04	6.87	−0.40	0.41	0.01
17	8.10	8.58	8.40	0.42	0.56	0.13
23	7.26	7.95	7.83	−0.22	0.29	0.43
24	7.32	7.89	7.74	0.23	0.43	0.42
30	7.66	8.63	8.21	1.11	1.43	1.52
34	9.05	8.55	8.50	1.32	1.47	1.47
35	9.21	8.68	8.13	1.83	1.36	1.53
38	8.20	7.95	8.54	1.38	1.15	1.98
56	8.80	8.17	8.10	2.31	2.04	1.90
57	7.37	8.38	8.36	2.06	2.91	3.00

[a] Calculated by using the best CoMSIA model.

properties as found by the CoMFA and CoMSIA analyses are illustrated together with exemplary ligands.

3.3.1. Models for pIC_{50}(PDE5). In Figure 3, the *steric properties* derived from the affinity (i.e., the activity) data are displayed for CoMFA (left) and CoMSIA (right). Areas indicated by green contours correspond to regions where steric occupancy with bulky groups should increase affinity. Areas encompassed by yellow isopleths should be sterically avoided; otherwise, re-

duced affinity can be expected. As it becomes immediately obvious, the CoMSIA method provides more contiguous contour diagrams,[28] which allows an easier interpretation of the correlation results mapped back onto the molecular structures. Furthermore, CoMSIA isocontour diagrams lie within regions occupied by the ligands, whereas CoMFA contours highlight those areas where the ligand would interact with a possible environment. Yet, the combined use of different methods enables one to verify the convergence of the results or to complement either conclusion.[44] As shown in Figure 3 (left), compound **20**, a very potent ligand for PDE5, orients its phenyl into a green area, which was in agreement with findings from the CoMSIA. Meanwhile, as shown in Figure 3 (right), the rather low binding affinity values of compound **5** could be due to the orientation of its benzyl group into a yellow area, which was not shown by CoMFA. This finding can be understood in considering the low activity of compounds such as **1**, **2**, **15**, and **16**. These compounds all orient their benzyl group into this yellow area. In addition, the green area near *Z*-position shown in Figure 3 (left) indicates that a bulky group at *Z*-position may increase the affinity, which is in agreement with findings from the CoMSIA model (Fig. 3, right). However, the yellow area near the *Y*-position indicates a bulky group at *Y*-position is disfavored for the activity, which is not shown in the CoMSIA model. This observation is confirmed by the fact that hydroxyl derivatives at *Y*-position always display inhibitory activity higher than that of methoxyl derivatives.

The above discussion indicated that exploiting the results of both approaches leads to a better interpretation at the 3D level of the QSAR and QSSR. In any case, however, it must be remembered that all of the features

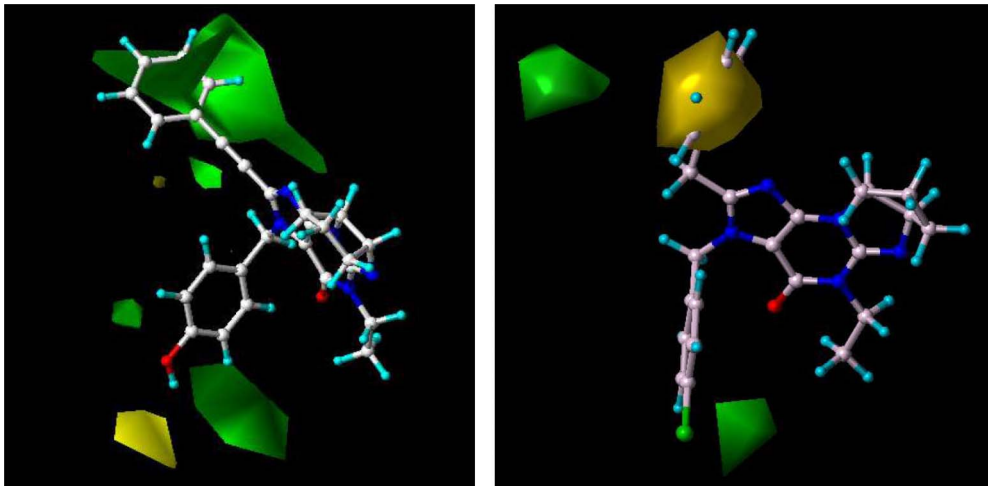

Figure 3. Contour maps of pIC_{50}(PDE5) models for steric field as obtained by CoMFA (left) and CoMSIA (right) analyses. Green isopleths enclose areas where steric bulk will enhance affinity. Yellow contours highlighted areas that should be kept unoccupied, otherwise affinity will decrease. These maps are demonstrated by the highly active compound **20** (left) and low active compound **5** (right). Compound **20** orients its phenyl group into a green area, while the benzyl group of compound **5** reaches a yellow highlighted area.

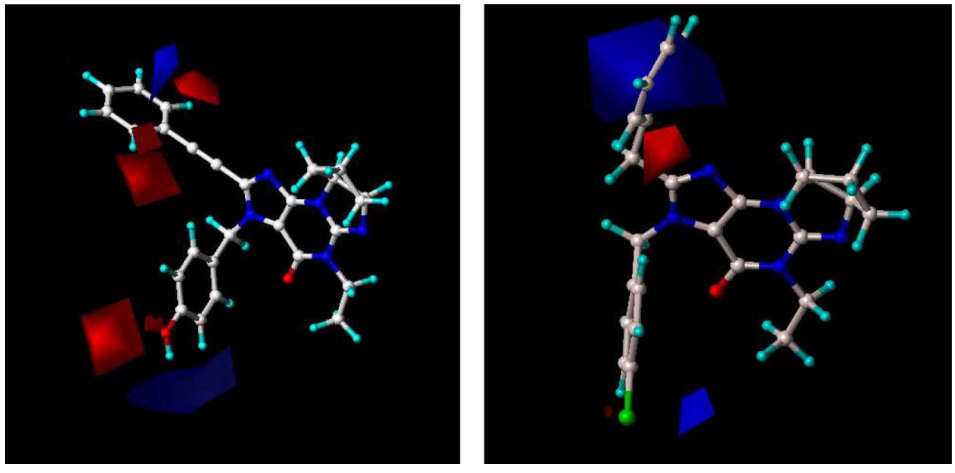

Figure 4. Contour maps of pIC_{50}(PDE5) models for electrostatic field as obtained by CoMFA (left) and CoMSIA (right) analyses. Red isopleths enclose areas where an increase of negative charge will enhance affinity, whereas in blue-contoured areas increase of positive charge is favorable for binding properties. These maps are demonstrated by the highly active compound **20** (left) and low active compound **5** (right). The phenyl group of compound **20** is near the red areas, while compound **5** orients its benzyl group into a blue highlighted area.

derived from a comparative molecular field analysis are only a mirror of the structural variations inherently present in the selected data set. Accordingly, selecting another structurally deviating data set may result in different features leading to alternative conclusions.

Maps for *electrostatic properties* are shown in Figure 4 with compound **20** as an example for a high-activity inhibitor and compound **5** as an example for a poor inhibitor. Negatively charged groups at the *Y*-position of phenyl group and electron-withdrawing substituents at *X*-position are favored. A blue isopleth above the phenyl ring system of compound **20**, which was occupied by the benzyl group of compound **5** as shown in Figure 4 (right), is representing an area where a positive charge is favored.

The contour plot for the *hydrogen-bond acceptor properties* (Fig. 5) shows an area in magenta that represents regions of proton donors on the receptor site. This area is near the hydroxyl oxygen at *Y*-position. This is in line with the docking result of compound **20** into the active site of the enzyme, which shows a hydrogen-bond formation between this oxygen and the amino acid residue of the binding site. This finding can account for the fact that a hydrogen-bond acceptor at *Y*-position is essential for the observed high activity of these compounds. The low activity of compound **5** is due to the fact that it does not have a hydrogen-bond acceptor near this magenta area.

3.3.2. Models for $\log IC_{50}$(PDE6/5). Figure 6 clearly indicates that the steric properties of cyclic guanine

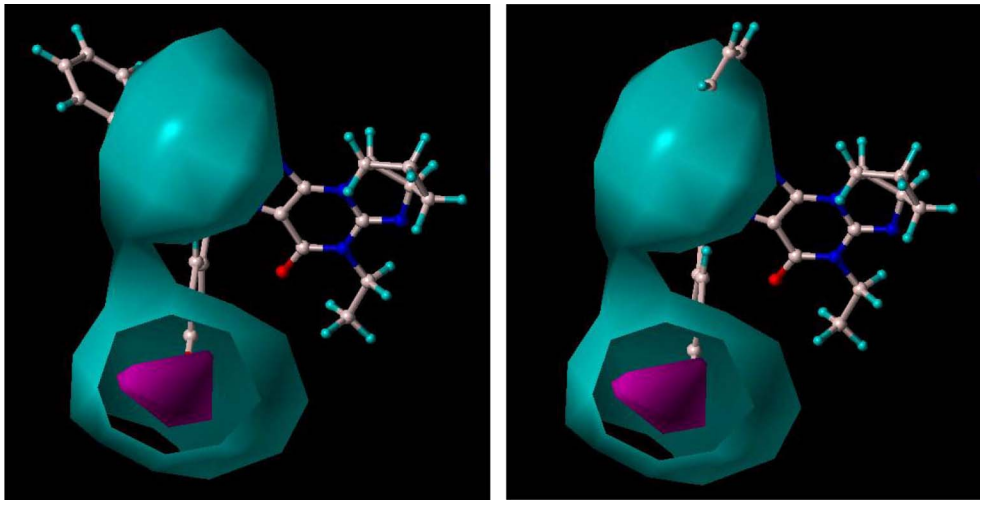

Figure 5. Contour maps of pIC_{50}(PDE5) models for hydrogen-bond acceptor field as obtained by CoMSIA analyses. Isopleths in magenta represent regions of hydrogen-bond donors on the receptor site. These maps are demonstrated by the highly active compound **20** (left) and low active compound **5** (right). The oxygen of hydroxyl group at *Y*-position of compound **20** is oriented toward these areas, while compound **5** does not have hydrogen-bond acceptor atom near these magenta area.

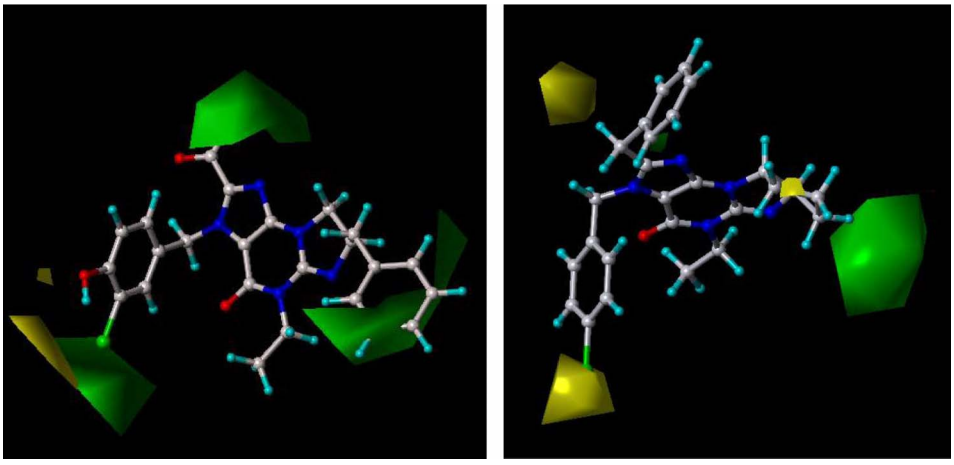

Figure 6. Contour maps of $\log IC_{50}$(PDE6/5) models for steric field as obtained by CoMFA (left) and CoMSIA (right) analyses. Green isopleths enclose areas where steric bulk will enhance the selectivity. Yellow contours highlighted areas that should be kept unoccupied, otherwise the selectivity will decrease. These maps are demonstrated by the highly selective compound **52** (left) and low selective compound **5** (right). Compound **52** orients its phenyl group into a green area, while compound **5** does not reach its any part into a green area.

derivatives play an important role in the selectivity. Compound **52**, a highly selective inhibitor of PDE5 against PDE6, inserted its benzyl group at C-8 position into a green area. It suggests that this moiety is an important recognition element for binding with PDE5, whereas the corresponding pocket in PDE6 is relatively limited. Furthermore, the combined information obtained from both Figures 3 and 6 suggests that the space of binding site for group at *Y*-position is limited, which explains why compounds with a hydroxyl group at *Y*-position are always more active and more selective than that bearing a methoxyl group. The combined information obtained from both Figures 4 and 7 suggests that compounds bearing (partially) positively charged substituents at *X*-position could increase not only the activity, but also the selectivity, whereas groups with partial negative charge at *Z*-position could also help to increase the activity and selectivity. The hydrophobic effect on the selectivity can be drawn from Figure 8 (left), suggesting that occupation of *Z*-position by a hydrophobic group would increase the selectivity, whereas a hydrophilic group at *X*-position is crucial for a highly selective inhibitor. The similarity of the contour plots of hydrogen-bond acceptor properties between the pIC_{50}(PDE5) and $\log IC_{50}$(PDE6/5) models reveals that the hydrogen bonding interaction of the ligand with PDE5 is different from that with PDE6. Oxygen at *Y*-position acts as a hydrogen-bond acceptor interacting with PDE5. On the other hand, there is probably no hydrogen bonding interaction of this oxygen with PDE6. Hence, the presence of hydrogen bonding acceptor at *Y*-position is favorable not only for the inhibitory activity against PDE5, but also for the selectivity against PDE6.

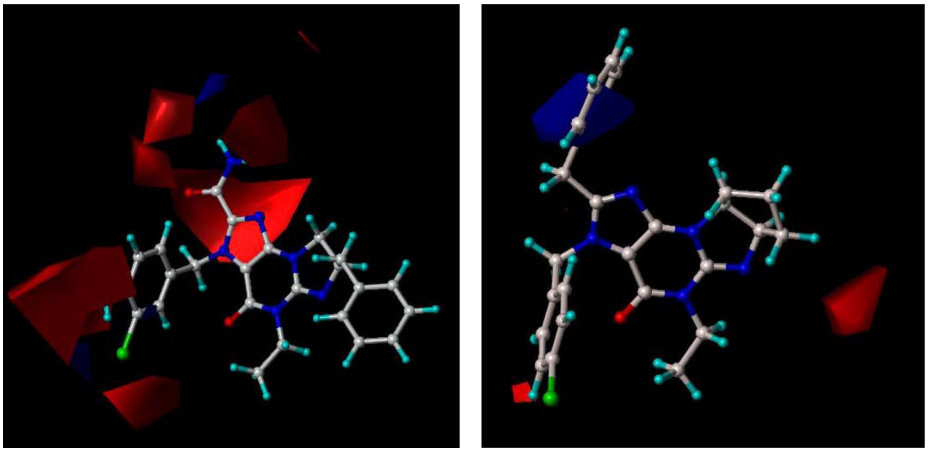

Figure 7. Contour maps of $\log IC_{50}$(PDE6/5) models for electrostatic field as obtained by CoMFA (left) and CoMSIA (right) analyses. Red isopleths enclose areas where an increase of negative charge will enhance selectivity, whereas in blue-contoured areas increase of positive charge is favorable for selectivity. These maps are demonstrated by the highly selective compound **52** (left) and low selective compound **5** (right). The benzyl group of compound **5** is across the blue area.

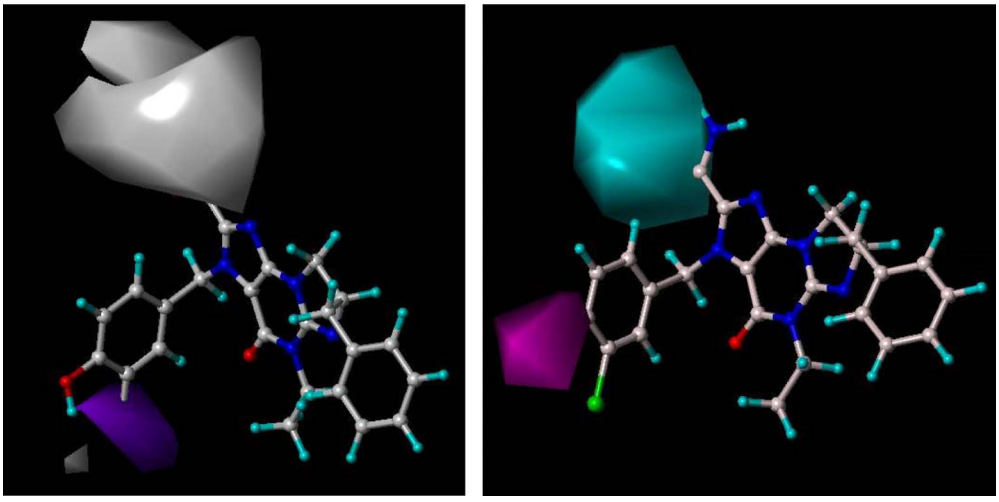

Figure 8. Contour maps of $\log IC_{50}$(PDE6/5) models for hydrophobic (left) and hydrogen-bond acceptor (right) field as obtained by CoMSIA analyses. For hydrophobic properties, purple isopleths encompass regions favorable for hydrophobic groups. In white-contoured areas, more hydrophilic groups are favorable for selectivity. For hydrogen-bond acceptor field, isopleths in magenta represent regions of hydrogen-bond donors on the receptor site. These maps are demonstrated by the highly selective inhibitor (compound **52**).

3.4. Comparison of QSAR models with the X-ray crystal structure of PDE5

The three-dimensional crystal structures of the catalytic domain of human PDE5 complexed with three drug molecules indicate that the PDE5 active site is located at the center of the C-terminal helical bundle domain.[21] The substrate binding pocket of PDE5 is composed of four subsites: a metal binding site (M site), core pocket (Q pocket), hydrophobic pocket (H pocket), and lid region (L region).[21] Our docking results indicate that the title compounds do not interact directly with the M site, which is consistent with the X-ray crystal structures. A common hydrogen bond between the nitrogen of the amine group of the Glu817 side chain and the carbonyl oxygen of the title compounds revealed by the X-ray crystal structures was also shown in our docked PDE5-ligand structures. The benzyl group at the N-3 position fits into the hydrophobic H pocket, and the oxygen atom at *Y*-position may form a hydrogen bond via a water-bridge with the amino acid residues in the H pocket, which is consistent with the QSAR results that *Y*-position of the title compounds is an important H-bonding site. The docking results demonstrate that the benzyl group at *X*-position of the ligand is surrounded by Tyr664, Ala823, and Gly819 residues in the L region of PDE5. The QSAR results reveal that this benzyl group is surrounded by a yellow region, which is consistent with the docked structures that the L region of PDE5 is a very limited pocket because residues #662 to #664 act as a 'lid' over the pocket. The 'lid' narrows the entrance to the PDE5 active site. In addition, our QSAR results suggest that the benzyl group at the position-8 of the ligand stays in an important site discriminating between PDE5 and PDE6, which is consistent with the docked PDE5-ligand structures showing an ample space surrounding the benzyl group of the ligand. Thus, both the QSAR analysis and molecular docking consistently suggest that the introduction of a bulky group into this site should increase the PDE5 inhibitory activity and reduce the PDE6 inhibitory activity. In short, our QSAR results are in agreement with the available X-ray crystal structures of PDE5.

4. Conclusion

Understanding intermolecular interactions of cyclic guanine derivatives with phosphodiesterase-5 (PDE5) and PDE6 is achieved by performing molecular docking, 3D-QSAR, and 3D-QSSR analyses. The use of molecular conformations of the compounds derived from molecular docking led to satisfactory 3D-QSAR and 3D-QSSR models (with high cross-validation correlation coefficient q^2 and conventional correlation coefficient r^2 values) for predicting the inhibitory activity against PDE5 and the selectivity against PDE6. The high q^2 and r^2 values, along with further testing, indicate that the obtained QSAR and QSSR models should be valuable in predicting both the inhibitory activity and selectivity of cyclic guanine derivatives against these protein targets. A set of 3D contour plots drawn based on the 3D-QSAR and QSSR models reveals some useful clues to improve the inhibitory activity and selectivity by modifying structures of the compounds. Comparison of QSAR models with the X-ray crystal structures of PDE5 indicates that cyclic guanine derivatives have a similar binding mode as sildenafil and a binding site for PDE5 and PDE6 selectivity was revealed by QSSR analysis. It has been demonstrated that both the steric and electrostatic factors should appropriately be taken into account for designing novel PDE5 inhibitors expected to have the higher inhibitory activity and higher selectivity.

Acknowledgments

This research was supported by the College of Pharmacy and the Center for Computational Sciences (CCS) at University of Kentucky. The work was performed when GFY worked in CGZ's laboratory at University of Kentucky as a visiting scientist. The authors acknowledge CCS at University of Kentucky for supercomputing time on Superdome (a shared-memory supercomputer, with 4 nodes and 256 processors).

References and notes

1. Francis, S. H.; Lincoln, T. M.; Corbin, J. D. *J. Biol. Chem.* **1980**, *255*, 620–626.
2. Thomas, M. K.; Francis, S. H.; Corbin, J. D. *J. Biol. Chem.* **1990**, *265*, 14964–14970.
3. Francis, S. H.; Turko, I. V.; Corbin, J. D. *Prog. Nucleic Acid Res. Mol. Biol.* **2001**, *65*, 1–52.
4. Liu, L.; Underwood, T.; Li, H.; Pamukcu, R.; Thompson, W. J. *Cell Signal* **2002**, *14*, 45–51.
5. Zoraghi, R.; Corbin, J. D.; Francis, S. H. *Mol. Pharmacol.* **2004**, *65*, 267–278.
6. Corbin, J. D.; Francis, S. H. *J. Biol. Chem.* **1999**, *274*, 13729–13732.
7. Blount, M. A.; Beasley, A.; Zoraghi, R.; Sekhar, K. R.; Bessay, E. P.; Francis, S. H.; Corbin, J. D. *Mol. Pharmacol.* **2004**, *66*, 144–152.
8. Corbin, J. D.; Francis, S. H. *Int. J. Clin. Pract.* **2002**, *56*, 453–459.
9. Sebkhi, A.; Strange, J. W.; Phillips, S. C.; Wharton, J.; Wilkins, M. R. *Circulation* **2003**, *107*, 3230–3235.
10. Burnett, A. L.; Lowenstein, C. J.; Bredt, D. S.; Chang, T. S.; Snyder, S. H. *Science* **1992**, *257*, 401–403.
11. Burnett, A. L. *J. Androl.* **2002**, *23*, S20–S26.
12. Lincoln, T. M. *Mol. Pharm.* **2004**, *66*, 11–12.
13. Rotella, D. P. *Nat. Rew. Drug Discov.* **2002**, *1*, 674–682.
14. Burnett, A. L. *Eur. Urol.* **2004**, *46*, 9–14.
15. Kukreja, R. C.; Ockaili, R.; Salloum, F.; Yin, C.; Hawkins, J.; Das, A.; Xi, L. *J. Mol. Cell Cardiol.* **2004**, *36*, 165–173.
16. Abdel-Hamid, I. A. *Drugs* **2004**, *64*, 13–26.
17. Bi, Y.; Stoy, P.; Adam, L.; He, B.; Krupinski, J.; Normandin, D.; Pongrac, R.; Seliger, L.; Watsonc, A.; Macora, J. E. *Bioorg. Med. Chem. Lett.* **2004**, *14*, 1577–1580.
18. Rotella, D. P.; Sun, Z.; Zhu, Y.; Krupinski, J.; Pongrac, R.; Seliger, L.; Normandin, D.; Macor, J. E. *J. Med. Chem.* **2000**, *43*, 1257–1263.
19. Haning, H.; Niewohner, U.; Schenke, T.; Es-Sayed, M.; Schmidt, G.; Lampea, T.; Bischoffb, E. *Bioorg. Med. Chem. Lett.* **2002**, *12*, 865–868.

20. Gresser, U.; Gleiter, C. H. *Eur. J. Med. Res.* **2002**, *7*, 435–446.
21. Sung, B. J.; Hwang, K. Y.; Jeon, Y. H.; Lee, J.; Heo, Y. S.; Kim, J. H.; Moon, J.; Yoon, J. M.; Hyun, Y. L.; Kim, E.; Eum, S. J.; Park, S. Y.; Lee, J. O.; Lee, T. G.; Ro, S.; Cho, J. M. *Nature* **2003**, *425*, 98–101.
22. Zhang, K. Y. J.; Card, G. L.; Suzuki, Y.; Artis, D. R.; Fong, D.; Gillette, S.; Hsieh, D.; Neiman, J.; West, B. L.; Zhang, C.; Milburn, M. V.; Kim, S. H.; Schlessinger, J.; Bollag, G. *Mol. Cell* **2004**, *15*, 279–286.
23. Cramer, R. D., III; Patterson, D. E.; Bunce, J. D. *J. Am. Chem. Soc.* **1988**, *110*, 5959–5967.
24. Kubinyi, H., Ed.; *3D-QSAR in Drug Design. Theory, Methods and Applications*; ESCOM: Leiden (NL), 1993.
25. Kubinyi, H., Folkers, G., Martin, Y. C., Eds.; *3D-QSAR in Drug Design. Volume 2. Ligand–Protein Interactions and Molecular Similarity*; Kluwer/ESCOM: Dordrecht (NL), 1997.
26. Kubinyi, H., Folkers, G., Martin, Y. C., Eds.; *3D-QSAR in Drug Design. Volume 3. Recent Advances*; Kluwer/ESCOM: Dordrecht (NL), 1998.
27. Klebe, G.; Abraham, U.; Mietzner, T. *J. Med. Chem.* **1994**, *37*, 4130–4146.
28. Bohm, M.; Sturzebecher, J.; Klebe, G. *J. Med. Chem.* **1999**, *42*, 458–477.
29. Bursi, R.; Sawa, M.; Hiramatsu, Y.; Kondo, H. *J. Med. Chem.* **2002**, *45*, 781–788.
30. Sun, W. S.; Park, Y. S.; Yoo, J.; Park, K. D.; Kim, S. H.; Kim, J. H.; Park, H. J. *J. Med. Chem.* **2003**, *46*, 5619–5627.
31. Kuo, C. L.; Assefa, H.; Kamath, S.; Brzozowski, Z.; Slawinski, J.; Saczewski, F.; Buolamwini, J. K.; Neamati, N. *J. Med. Chem.* **2004**, *47*, 385–399.
32. Ahn, H. S.; Bercovici, A.; Boykow, G.; Bronnenkant, A.; Chackalamannil, S.; Chow, J.; Cleven, R.; Cook, J.; Czarniecki, M.; Domalski, C.; Fawzi, A.; Green, M.; Gundes, A.; Ho, G.; Laudicina, M.; Lindo, N.; Ma, K.; Manna, M.; McKittrick, B.; Mirzai, B.; Nechuta, T.; Neustadt, B.; Puchalski, C.; Pula, K.; Silverman, L.; Smith, E.; Stamford, A.; Tedesco, R. P.; Tsai, H.; Tulshian, D.; Vaccaro, H.; Watkins, R. W.; Weng, X.; Witkowski, J. T.; Xia, Y.; Zhang, H. *J. Med. Chem.* **1997**, 2196–2210.
33. Ho, G. D.; Silverman, L.; Bercovici, A.; Puchalski, C.; Tulshian, D.; Xia, Y.; Czarniecki, M.; Green, M.; Cleven, R.; Zhang, H.; Fawzi, A. *Bioorg. Med. Chem. Lett.* **1999**, *9*, 7–12.
34. Pissarnitski, D. A.; Asberom, T.; Boyle, C. D.; Chackalamannil, S.; Chintala, M.; Clader, J. W.; Greenlee, W. J.; Hu, Y.; Kurowski, S.; Myers, J.; Palamanda, J.; Stamford, A. W.; Vemulapalli, S.; Wang, Y.; Wang, P.; Wu, P.; Xu, R. *Bioorg. Med. Chem. Lett.* **2004**, *14*, 1291–1294.
35. Morris, G. M.; Goodsell, D. S.; Halliday, R. S.; Huey, R.; Hart, W. E.; Belew, R. K.; Olson, A. J. *J. Comput. Chem.* **1998**, *19*, 1639–1662.
36. Zhan, C.-G.; Norberto de Souza, O.; Rittenhouse, R.; Ornstein, R. L. *J. Am. Chem. Soc.* **1999**, *121*, 7279–7282.
37. Koca, J.; Zhan, C.-G.; Rittenhouse, R.; Ornstein, R. L. *J. Am. Chem. Soc.* **2001**, *123*, 817–826.
38. Zheng, F.; Zhan, C.-G.; Ornstein, R. L. *J. Phys. Chem. B* **2002**, *106*, 717–722.
39. Koca, J.; Zhan, C.-G.; Rittenhouse, R. C.; Ornstein, R. L. *J. Comput. Chem.* **2003**, *24*, 368–378.
40. Zhan, C.-G.; Zheng, F. *J. Am. Chem. Soc.* **2001**, *123*, 2835–2838.
41. Stote, R. H.; Karplus, M. *Proteins* **1995**, *23*, 12–31.
42. Case, D. A.; Pearlman, D. A.; Caldwell, J. W.; Cheatham III, T. E.; Wang, J.; Ross, W. S.; Simmerling, C. L.; Darden, T. A.; Merz, K. M.; Stanton, R. V.; Cheng, A. L.; Vincent, J. J.; Crowley, M.; Tsui, V.; Gohlke, H.; Radmer, R. J.; Duan, Y.; Pitera, J.; Massova, I.; Seibel, G. L.; Singh, U. C.; Weiner, P. K.; Kollman, P. A. AMBER 7, University of California, San Francisco, **2002**.
43. Frisch, M. J.; Trucks, G. W.; Schlegel, H. B.; Scuseria, G. E.; Robb, M. A.; Cheeseman, J. R.; Montgomery, Jr., J. A.; Vreven, T.; Kudin, K. N.; Burant, J. C.; Millam, J. M.; Iyengar, S. S.; Tomasi, J.; Barone, V.; Mennucci, B.; Cossi, M.; Scalmani, G.; Rega, N.; Petersson, G. A.; Nakatsuji, H.; Hada, M.; Ehara, M.; Toyota, K.; Fukuda, R.; Hasegawa, J.; Ishida, M.; Nakajima, T.; Honda, Y.; Kitao, O.; Nakai, H.; Klene, M.; Li, X.; Knox, J. E.; Hratchian, H. P.; Cross, J. B.; Adamo, C.; Jaramillo, J.; Gomperts, R.; Stratmann, R. E.; Yazyev, O.; Austin, A. J.; Cammi, R.; Pomelli, C.; Ochterski, J. W.; Ayala, P. Y.; Morokuma, K.; Voth, G. A.; Salvador, P.; Dannenberg, J. J.; Zakrzewski, V. G.; Dapprich, S.; Daniels, A. D.; Strain, M. C.; Farkas, O.; Malick, D. K.; Rabuck, A. D.; Raghavachari, K.; Foresman, J. B.; Ortiz, J. V.; Cui, Q.; Baboul, A. G.; Clifford, S.; Cioslowski, J.; Stefanov, B. B.; Liu, G.; Liashenko, A.; Piskorz, P.; Komaromi, I.; Martin, R. L.; Fox, D. J.; Keith, T.; Al-Laham, M. A.; Peng, C. Y.; Nanayakkara, A.; Challacombe, M.; Gill, P. M. W.; Johnson, B.; Chen, W.; Wong, M. W.; Gonzalez, C.; Pople, J. A. *Gaussian 03*, Revision A.1, Gaussian, Inc., Pittsburgh, PA, **2003**.
44. Boulamwini, J. K.; Assefa, H. *J. Med. Chem.* **2002**, *45*, 841–852.